The Effects of Native Tissue Vascularity and Increased Anaerobic Tumor Metabolism by A.A. Patel et al.

Systems Biology DTC 2012

OSTI Phase 1: A Cellular Automaton Model of Early Tumor Growth and Invasion

Jackie Ang, Alexander Erlich, Robert Ross, Jonathan Brooks-Bartlett, James Mbewu

January 2013
University of Oxford

Contents

Chapter 1

Introduction

by Jackie Ang

Cancer is a major cause of death worldwide and is defined as unregulated cell growth within a structure known as a tumour. Tumour growth can be classified into distinct stages, which are hyperplasia, dysplasia, in situ carcinoma and finally invasive cancer. As tumours are made up of rapidly dividing cells, they require high amounts of oxygen and glucose for survival and cell division. This rapidly overwhelms the ability of normal blood vessels to provide these nutrients and leads to angiogenesis within the tumours. Also, as a consequence of hypoxia within the tumour, cells switch to using anaerobic respiration and release lactic acid into the extracellular environment. This causes a decrease in the pH in the environment within and around the tumour and also leads to necrosis. While the initiation of this switch to anaerobic respiration is often said to be an adaptation to the hypoxic environment, some investigators have found that it occurs even with an adequate oxygen supply and is a phenotypic consequence [2][5][6].

The resulting decrease in the environmental pH has deleterious effects on normal tissue as they have a much higher pH threshold for viability compared to tumour cells. Also, the decreased pH stimulates the production of enzymes which degrade the extracellular matrix and causes the loosening of gap junctions between cells. The degradation of extracellular matrix then allows the invasion of tumour cells into the host tissue. A discrete mathematical model involving all of these parameters as well as diffusion is thus useful for studying the interaction of tumour cells with its surrounding tissue as well as for the investigation of the changes within the microenvironment around the developing tumour.

Cellular automata has a long history of usage to model the growth and development of tumours. In this investigation by A.A. Patel et al, a hybrid cellular automaton was used to model an early stage of tumour growth. The cellular automaton assumes tumour avascularity and a random distribution of blood vessels in a tissue, which is true for pre-angiogenic tumours. The model includes variables for glucose and lactic acid concentration. It however, does not include a variable for oxygen concentration as the author is focusing on the effects of acidification of the microenvironment rather than hypoxia. It was shown that anaerobic respiration in tumour cells persists even in high levels of oxygen and tumour cell viability is independent of oxygen levels [3].

Chapter 2

Methods

by Jackie Ang et al.

2.1 Setup of Cellular Automaton

First, a two-dimensional cellular automaton was created to model this tumour growth. This was made up of a N by M array of elements with a value corresponding to the state of each point. This state describes the occupation status of each point, with values corresponding to active normal cell, quiescent normal cell, necrotic normal cell, active tumour cell, quiescent tumour cell, necrotic tumor cell and blood vessel. Although both necrotic normal cells and necrotic tumor cells are effectively vacant elements (as referred to by Patel et al, in [4]) we made the distinction in the model so we could measure the radius of gyration of the tumor cells which required the use of all states of tumor cells including the necrotic state. Active cells are allowed to divide whereas quiescent cells are not.

Two other N by M arrays of elements with positional conservation to the first array were also created to represent the glucose and lactic acid concentrations of each individual automaton element. This differs from the authors in that they created a matrix of state-vectors each containing four components which correspond to the same variables, but leads to similar results.

In [4] the authors also mentioned one of the four above components as ghost values used only on elements occupied by vessels to enforce gradient boundary conditions at the four walls of the vessels. However, this has been covered In our program by fixing the glucose and lactic acid concentrations in elements occupied by vessels and not allowing them to change during the process of running the cellular automaton.

The cellular automaton was randomly populated with microvessels using a user defined microvessel density ϕ_v where

$$\phi_v = \frac{N_v}{N^2} \tag{2.1}$$

where N_v is the number of vessel elements inside the automaton.

The program situates the vessel elements randomly, subject to the condition that any given tumour cell or normal cell element can only border a maximum of one vessel element. This is because if a cell element borders two or more vessels, the value of the glucose and

lactic concentrations would be too strongly affected by the multiple boundary conditions imposed by the vessels.

All other elements within the cellular automaton were then populated with active normal cells. Following this, a disc shaped group of active tumour cells with a user defined diameter is introduced in the centre of the automaton grid, replacing any normal cells or vessels previously there.

The other two N by M arrays are then populated with starting values for glucose and lactic acid concentrations. For glucose concentrations, a glucose profile is generated based on the diffusion equations and the position of the vessels before the insertion of any non-vessel cells. The glucose concentration at vessels however, is kept constant at $G_s = 5.0mM$. The lactic acid concentration is initialised at all elements at $H_s = 3.98 \cdot 10^{-5}mM$. This lactic acid concentration corresponds to a pH of 7.4 in the extracellular environment.

2.2 Rules of Cellular Automaton

There are several rules for this cellular automaton as described below

1. Elements occupied by microvessels do not change in status, glucose and lactic acid concentrations in the entire simulation.

2. Normal cells and tumour cells cannot evolve into other forms of cells. They can only change status from active to quiescent or vice versa. They may also die and this results in a vacant element (represented in code as a necrotic normal cell or a necrotic tumor cell if they were previously a normal or tumor cell respectively).

3. If the occupancy of an automaton element is with a normal cell or tumour cell, after each updating of glucose and lactic acid concentrations of elements, if the local glucose concentration is below G_N^D or G_T^D, which were both defined to be 2.5mM, the cell dies and the occupancy becomes a corresponding necrotic cell.

4. If there is enough glucose, the local lactic acid concentration of the individual elements is then checked. For normal cells, if the local lactic acid concentration exceeds H_N^D, defined as $1.58 \cdot 10^{-4}mM$ (pH 6.8), it becomes necrotic. Otherwise if the concentration of lactic acid is between H_N^Q, defined as $7.94X10 - 5mM$ (pH 7.1) and H_N^D, the cell survives but becomes quiescent. For tumour cells, if the local lactic acid concentration is above H_D^T, defined as $1 \cdot 10^{-3}mM$ (pH 6.0), it dies. Otherwise if the concentration of lactic acid is between H_T^Q, defined as $3.98 \cdot 10^{-4}$ (pH 6.4) and H_T^D, it survives but becomes quiescent. For a normal cell, if the local lactic acid concentration exceeds H_N^Q then the normal cell will become active. Similarly for the tumor cell, if the local lactic acid concentration exceeds H_T^Q then the normal cell will become active.

5. Any cells that are now in an active state will be allowed to divide. This can only occur if there is a vacant element adjacent to the cell and can only occur once per cell even if there is more than one vacant element adjacent to the cell. If there is more than one vacant neighbour, the neighbouring element with the highest glucose concentration will receive the daughter cell.

2.3 Running the Simulation

While there is a large disparity in the timescales of cell division(10^2 hours) and diffusion of glucose and lactic acid($1 - 10$ seconds), it has been attempted to reconcile this difference by stating that the distributions of nutrients and by products do not change after reaching a steady state quickly and changes in cell status can be treated as perturbations on the chemical distributions.

The problem of all cells responding simultaneously to changes in chemical distributions has also been addressed by advancing the automaton in a series of sub-generations. A generation is defined as the time taken for all the elements within the automaton to be updated. For the purpose of the simulations, the user defines number of subgenerations and hence the random fraction of cells that get updated each subgeneration (denoted by f) is calculated accordingly.

Importantly, at the start of a subgeneration a death_matrix is initialised. This stores the composition of the state_matrix, i.e. cell types in cellular automaton, at the start of each subgeneration.

Within each sub generation, a random subset $1/f$ of non-vessel automaton elements are selected for updating. This is acheived by iterating through $1/f$ of a randomised $N*M$ vector consisting of a number corresponding to each cell. This randomised $N*M$ vector is reinitialised at the beginning of every generation. The update takes the following order:

1. The entire glucose and lactic acid fields are updated according to the solution of the equilibrium boundary value problems.

2. The state of the selected subgeneration of cells is then updated as quiescient, necrotic or active depending on the surrounding (cell right, left, up and down) pH and glucose fields.

3. Following this, the death_matrix, a representation of the state_matrix at the start of the subgeneration is used to decide whether active cells from the current subgeneration state_matrix can divide into free space created in previous subgenerations. This scheme means cells that have died in the current subgeneration cannot be occupied in the same subgeneration. At the end of the subgeneration the death matrix is updated to the current state_matrix, i.e. with the subgeneration changes, meaning that active cells in the next subgeneration are able to divide into the vacant grid elements.

2.4 The GUI

The graphical user interface (GUI) was made to visualise the results and is intended to summarise the most useful and important information in the simulation (see figure 2.1). When the "cancerModelGUI" script is run the GUI appears on screen with a list of the parameters on the right hand side of the screen. The user can input the parameters into the relevant text box in the GUI and then click the "RUN" button to see the results. The left hand side of the GUI contains the subplots that show the visual data produced when the code is run. The top left subplot shows the resulting state matrix after each full

generation. The subplot on the top right handside of the GUI shows the radius of gyration of the tumor against the number of full generations that the simulation has completed (the radius of gyration is explained in section 2.10). The subplots on the bottom left and bottom right show the glucose concentration and the pH on the grid respectively. These subplots are updated every subgeneration.

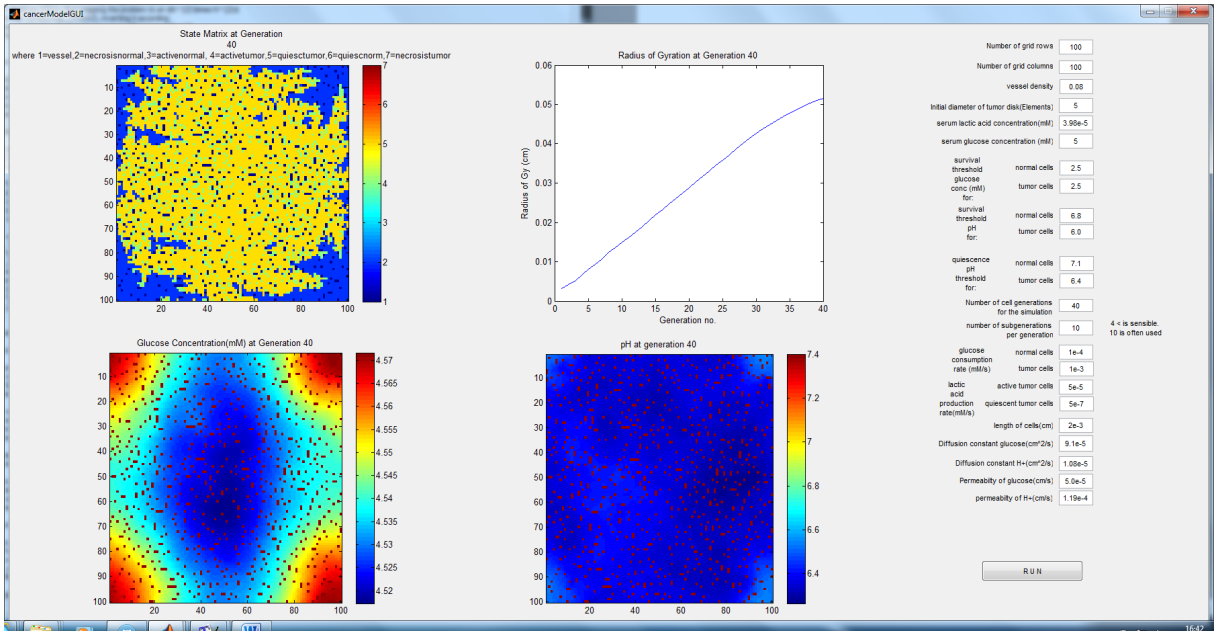

Figure 2.1: Figure showing the GUI that has been created to display the results of the simulation

2.5 Glucose Inversion Problem

The problem is to obtain a spatial solution of a steady state diffusion equation

$$D_G \nabla^2 G(\mathbf{r}) - k(\mathbf{r}) G(\mathbf{r}) = 0 \tag{2.2}$$

for the glucose concentration matrix G. The glucose consumption rates are stored in the matrix k as constants (we shall give further information on this shortly). Here, D_G is the glucose diffusion constant (a scalar) and G, K are an $N \times N$ matrices[1]. We want to solve this equation for the glucose concentration $G(\mathbf{r})$, i.e. on an $N \times N$ domain, with periodic boundary conditions.

Let us define G in $\mathbb{R}^{N \times N}$, so in an orthonormal basis $\{\mathbf{e}_k\}$ we obtain

$$G = G_{i,j} \mathbf{e}_i \otimes \mathbf{e}_j \tag{2.3}$$

which is a summation over indices i, j (summation convention). The periodic boundary condtions for the first index are

$$\begin{aligned} G_{0j} &\longrightarrow G_{Nj} \\ G_{N+1,\,j} &\longrightarrow G_{1,\,j} \end{aligned}$$

[1]It is slightly odd that the authors choose a lower case symbol for a matrix but we shall stick to their notation. After all, $k\,G$ is a matrix product (summation over 2 indices). The authors might have decided for this notation because$k$ is a matrix of constants, i.e. $k = k(\mathbf{r})$ but $k_{ij} \neq k_{ij}(\mathbf{r})$.

and the same for the other index. The cell distribution is expressed through the matrix $k(\mathbf{r})$ in terms of their glucose consumption rates

$$k(\mathbf{r}) = \begin{cases} k_N & \forall \mathbf{r} = \text{Normal Cells} \qquad 1 \cdot 10^{-6}/s < k_N < 5 \cdot 10^{-4}/s \\ k_T & \forall \mathbf{r} = \text{Tumor Cells} \qquad 1 \cdot 10^{-5}/s < k_T < 1 \cdot 10^{-3}/s \\ 0 & \forall \mathbf{r} = \text{Vacant Cells} \qquad \text{no vacant cells at simulation startup} \\ 0 & \forall \mathbf{r} = \text{Vessel Cells} \end{cases} \tag{2.4}$$

The discretisation of (2.2) in terms of finite differences can be written as

$$\frac{G_{i+1,j} + G_{i-1,j} + G_{i,j+1} + G_{i,j-1} - 4G_{i,j}}{\Delta^2} - \frac{k_{i,j} G_{i,j}}{D_G} = 0 \tag{2.5}$$

where the above mentioned diffusion constant is approximately $D_G \approx 9.1 \cdot 10^{-5} cm^2/s$ and an automaton element is roughly of the size $\Delta^2 \approx (20\mu)^2$ which is a rough approximation for cell size. At this point, we have set up the system fully except for the vessel boundary conditions.

2.6 Vessel Boundary Conditions

The reason why 2.5 unfortunately cannot be written as a linear system $DG = K. * G^2$ is the vessel boundary conditions. If a vessel is placed at i, j (corresponding to $k_{ij} = 0$ since no vacant cells are allowed at simulation startup, see 2.4) then G_{ij} cannot be accessed and therefore 2.5 must be modified.

If, for instance, a cell (i, j) has a vessel to its right $(i, j-1)$ then it cannot access this normal direction. Consequently, we will treat this cell (at the boundary to a vessel to its left) in terms of finite differences[3] as

$$G_{i+1,j} + G_{i-1,j} + G_{i,j+1} - 4G_{i,j} - \left(3 + \frac{\Delta^2 k_{i,j} + q_G \Delta}{D_G}\right) G_{i,j} = -\frac{q_G \Delta}{D_G} G_S \tag{2.6}$$

where G_S is the serum glucose value $G_S \approx 5.0 mM$ and the permeability of the vessel wall is $q_G \approx 3.0 \cdot 10^{-5} cm/s$. Similarly, for a cell (i, j) with a vessel at the above / below normal direction, the indices $(i-1,\ j)\ /\ (i+1,\ j)$ are not accessible and eqn. 2.6 must be adapted accordingly.

2.7 Numerical Approach

We are interested in obtaining the elements of the glucose concentration matrix

$$G \in \mathbb{R}^{N \times N} \tag{2.7}$$

from the values of the glucose consumption rate matrix

$$k \in \mathbb{R}^{N \times N} \tag{2.8}$$

[2]meaning $(DG)_{ij} = D_{im} G_{mj}$ and $(K. * G)_{ij} = K_{ij} G_{ij}$, not sure how to express that mathematically, I am just using Matlab element wise notation.

[3]There is an error in the paper, cf. eq. (13) on page 322.

specified in 2.4.

In order to be able to manipulate elements G_{ij} individually, we construct an $N^2 \times N^2$ matrix D and reformulate the $N \times N$ matrix G into a column vector $\mathbf{g}$ with N^2 elements. More precisely, if

$$G = (\mathbf{G}_1 \quad \mathbf{G}_2 \quad \cdots \quad \mathbf{G}_N) \tag{2.9}$$

we choose

$$\mathbf{g} = \begin{pmatrix} \mathbf{G}_1 \\ \mathbf{G}_2 \\ \vdots \\ \mathbf{G}_N \end{pmatrix} \qquad \mathbf{g} \in \mathbb{R}^{N^2} \tag{2.10}$$

and $D \in \mathbb{R}^{N^2 \times N^2}$, $\mathbf{b} \in \mathbb{R}^{N^2}$, $\mathbf{k} \in \mathbb{R}^{N^2}$ where the latter two are yet to be constructed. As a result, we can formulate a linear matrix inversion problem

$$D\mathbf{g} = \mathbf{b} \qquad \mathbf{g} = D^{-1}\mathbf{b} \tag{2.11}$$

which will be a solution to 2.5 coupled to 2.6. In components, the problem reads

$$\underbrace{\begin{pmatrix} D_{11} & \cdots & D_{N^2 1} \\ & & \\ \vdots & & \vdots \\ & & \\ D_{N^2 1} & \cdots & D_{N^2 N^2} \end{pmatrix}}_{N^2 \times N^2} \begin{pmatrix} G_{11} \\ \vdots \\ G_{N1} \\ G_{12} \\ \vdots \\ G_{NN} \end{pmatrix} = \begin{pmatrix} \mathbf{G}_1 \\ \mathbf{G}_2 \\ \\ \vdots \\ \\ \mathbf{G}_N \end{pmatrix} \tag{2.12}$$

A map 1-to-1 map between $G \in \mathbb{R}^{N \times N}$ and $\mathbf{g} \in \mathbb{R}^{N^2}$ can be worked out. If i, j are the indices of G and c is the element number of $\mathbf{g}$, we get routines

$$\texttt{function C} \;=\; \texttt{CfromIJ(I, J, N)} \tag{2.13}$$

$$\texttt{function[I, J]} \;=\; \texttt{IJfromC(C, N)} \tag{2.14}$$

In simple terms, the goal is in obtaining the glucose matrix $G \in \mathbb{R}^{N \times N}$ by first mapping the problem to an $N^2 \times N^2$ problem using the map 2.13, inverting it according to 2.11 and using the inverse 2.14 to obtain values for G.

2.8 Inversion Algorithm for the Glucose Matrix

1. Identify the indices i^*, j^* in k_{ij} (see eq. 2.8) on which a vessel is placed. Use the map 2.13 to obtain c^* and set

$$D_{c^*k} = \delta_{c^*k} \quad \Leftrightarrow \quad G_{i^*j^*} = 1 \tag{2.15}$$

   i.e. update one row in D.

2. Consider the four neighbors in the normal directions corresponding to indicies

$i^* - 1,\ j^*$	cell above vessel
$i^* + 1,\ j^*$	cell below vessel
$i^*,\ j^* - 1$	cell to the left of vessel
$i^*,\ j^* + 1$	cell to the right of vessel

   and update them taking account of the boundary conditions, i.e. by 2.6. This corresponds to updating rows in D. Also update $b_{c^*} = -q_G \Delta G_S / D_G$. Use 2.13 and 2.14 to switch between the representations.

3. Update all remaining cells according to 2.5, switching between representations by 2.13 and 2.14.

4. Find $D^{-1} \in \mathbb{R}^{N^2 \times N^2}$ by eqn. 2.11 and reshape D^{-1} into $G \in \mathbb{R}^{N \times N}$, 2.13 and 2.14 to convert.

2.9 Acid Profile

Even though the acid profile is just as important as the glucose concentration for the cellular automaton algorithm we shall treat it very briefly in this section because it is analogous to the glucose profile. To obtain the acid profile, we need to solve Poisson's equation

$$D_H \nabla^2 H(\mathbf{r}) + h(\mathbf{r}) = 0 \tag{2.16}$$

where the lactic acid diffusion constant is $D_H \approx 1.08 \cdot 10^{-5} \mathrm{cm}^2/s$ and $H(\mathbf{r})$ is the H^+ concentration. Similarly to $k(\mathbf{r})$ in eqn. 2.4, $h(\mathbf{r})$ is a matrix of constants $h = h(\mathbf{r})$ but $h_{ij} \neq h_{ij}(\mathbf{r})$. It is defined as

$$h(\mathbf{r}) = \begin{cases} \dot{H}_T^A & \forall \mathbf{r} = \text{Active tumor cells} \qquad 1 \cdot 10^{-5}\,\mathrm{mM/s} < \dot{H}_T^A < 1 \cdot 10^{-4}\,\mathrm{mM/s} \\ \dot{H}_T^Q & \forall \mathbf{r} = \text{Quiescent tumor cells} \qquad \dot{H}_T^Q = 5 \cdot 10^{-7}\,\mathrm{mM/s} \\ 0 & \forall \mathbf{r} \neq \text{Tumor cells} \end{cases} \tag{2.17}$$

where $\dot{H}_T^A$ and $\dot{H}_T^Q$ are the lactic acid production rates for active and quiescent tumor cells.

The solution of 2.16 with 2.17 can be obtained in absolute analogy to eqn. 2.5 and 2.6, with these slight adaptations:

1. Replace $D_G \to D_H$, $q_G \to q_H$, $G_S \to H_S$ where the lacitic acid diffusion constant D_H has been introduced previously, the vessel permeability to lacitic acid is $q_H \approx 1.19 \cdot 10^{-4}$ cm/s and the serum acid concentration (pH = 7.4) is $H_S = 3.98 \cdot 10^{-5}$ mM.

2. Replace $k_{i,j}G_{i,j} \to k_{i,j}$ because we are considering Poisson's equation now.

With these considerations, the algorithm described above for glucose applies to the lactic acid as well.

2.10 Calculating Tumour Size and Growth Rate

To analyse the model tumour size was characterised by its radius of gyration as was done by Patel *et al.* [4]. The tumour size was calculated including regions of active and quiescent tumour cells as well as tumour necrosis (i.e. where tumour cells have died). The radius of gyration R_G can be calculated as the square root of the second moment of the spatial distribution (J) divided by the total area of the spatial distribution (A), i.e.

$$R_G = \sqrt{\frac{J}{A}}, \tag{2.18}$$

returning a measure of the radius of the tumour (in this text reported in cm). The second moment of the spatial distribution can be calculated using the following formula:

$$J = \sum^{no.cells} J_{cell} + y^2 A_{cell}. \tag{2.19}$$

where $J_{cell} = \frac{l^4}{12}$ is the second moment of area of an individual square cell ($l = 20\mu m$ is the length of each cell), y is the distance in the y-direction to the centroid of the tumour and $A_cell = l^2$ is the area of each individual cell.

Note that in the original paper by Patel et al., the radius of gyration was stated as being square root of the second moment of area. However, this was clearly a mistake and their results corresponded to the above definition of the radius of gyration.

To analyse the growth rate of each tumour in each simulation, the radius of gyration for the last ten generations (out of a total of 40 generations) was analysed using linear regression to find the slope (i.e. tumour growth rate) of the regression line. This was generally an accurate representation of the growth rate since after an initial transient period, tumour size increased linearly (see Figure 3.1).

Chapter 3

Results

Figure 3.1 shows tumour size, as given by radius of gyration, with respect to generation number. Prior simulations allowed it to be gauged that tumour growth would only occur in the model above a lactic acid production of $4.75 \times 10^{-5} mM$. As can be seen, increasing acidity decreases growth rates in agreement with the Patel et.al paper (2001). This is because high lactic acid concentration kills normal cells while cancer cells have a higher resistance, and so therefore cancer cells are fitter in a more acidic environment.
Figure 3.2a shows growth rate vs. acid production, with the five plotted lines corresponding to different vessel distributions as given in the legend. It can be seen that increased vessel density increases growth rate generally, although not at all time points. In contrast, increasing acid production seems to affect growth rate but not in an easily understandable way. Figure 3.2b shows growth rate vs. vessel fraction, with the five plotted lines corresponding to different tumour acid production. It can be seen that as in figure 3.2a increasing vessel density increase growth rate regardless of lactic acid production rate. However, it appears that beyond a vessel density of 0.2 it becomes an inhibiting factor. In the [4] paper this in confirmed with growth rate decreasing with beyond a certain vessel density threshold.

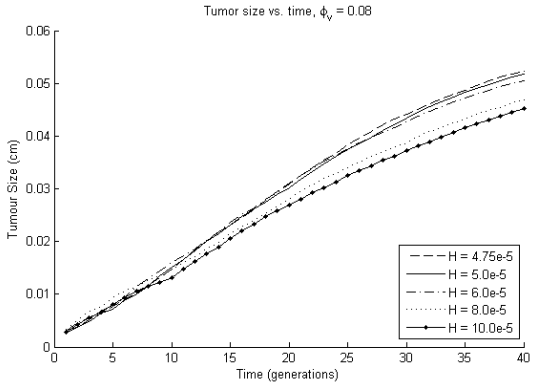

Figure 3.1: Graph showing the tumour size against the number of generations in the simulation

As can be seen from Figure 3.3 the glucose concentration does not vary a great deal in magnitude. In fact, the glucose level at which cell death occurs of $2.5mM$ (G_D and G_T) in the cellular automaton rules was never reached in our simulation. This is in correspondence with results of [4] and indicates that cells never die because of lack glucose, but only because of acidosis (high acid concentration). The glucose concentration does affect the

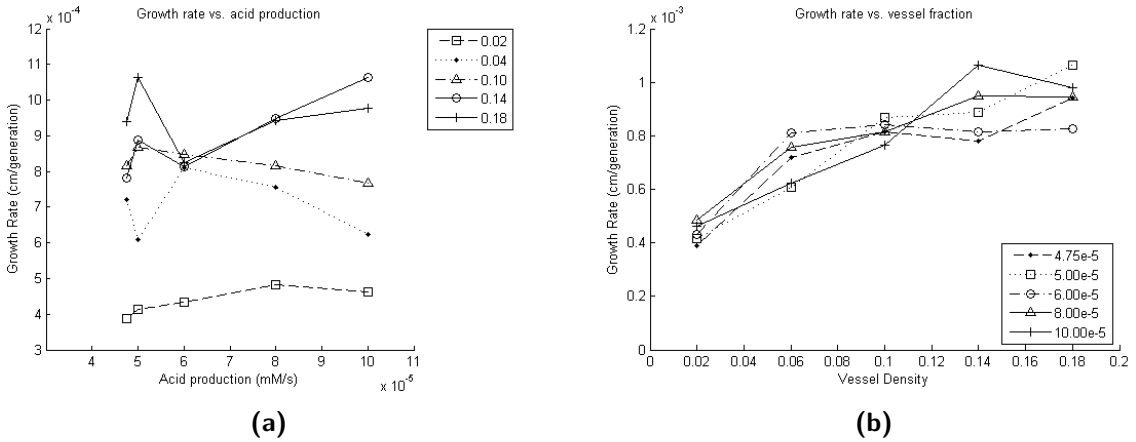

Figure 3.2: Figure (a) shows a graph showing the growth rate of the tumour vs the lactic acid production of the tumour cells. The results were plotted using different values for the vessel density in each simulation given in the legend. Figure (b) shows a graph showing the growth rate of the tumour vs the vessel density. The results were plotted using different values for the lactic acid production for the tumour cells in each simulation given in the legend.

simulation however, by controlling the direction in which cells divide in the automaton rules. This may be the cause of distinct cross shaped tumours for selected parameters.

Another feature of tumour growth is that the tumour inhibits its own growth by creating a high pH in and around itself. This can be seen in Figure 3.3 where the interior of the tumour is quiescent (coloured yellow) while at the outside of the tumour the cells are active and dividing (coloured green). Another thing to note is that in the interior, close to vessels (coloured blue), there are a number of active cells. This is because at these locations the pH is increased due to the proximity to the vessels which have a high pH and do not inactivate the tumour cells.

Also noticeable in the plots of cell state is the ring of dead cells in which tumour cells divide as well as a ring of quiescent normal cells. The ring of dead cells, termed the hypocellular gap, has been reproduced as predicted by Gatenby *et al.* [1] as well as in the paper this work was based on.

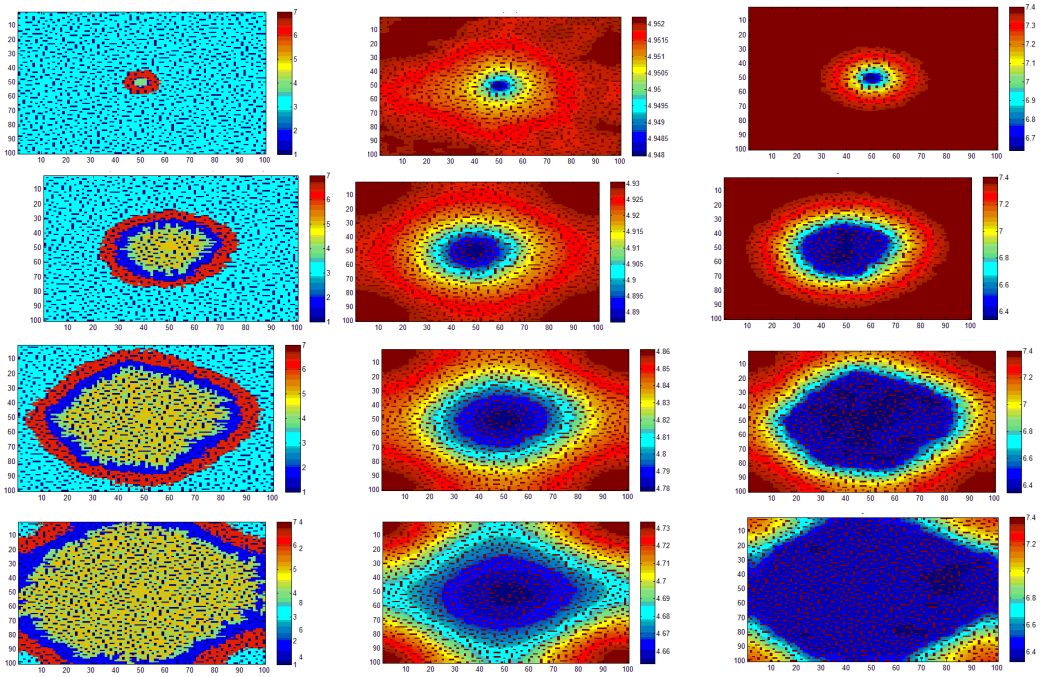

Figure 3.3: The temporal evolution of a tumour using the model described in this text (with parameters $\phi_v = 0.18$, and $H_T^A = 4.75 \times 10^-5 mM/s$) with 100×100 automaton elements. In the first column the cell state is shown, with numbers corresponding to 1) vessel, 2) dead normal cell, 3) active normal cell, 4) active tumour cell, 5) quiescent tumour cell, 6) quiescent tumour cell and 7) dead tumour cell. The tumour is plotted at generations 1, 11, 21 and 31. The hypocellular ring is clearing visible infront of the advancing tumour.

Chapter 4

Discussion

4.1 Problems Faced with Original Paper and Differences

We faced a few problems in the interpretation of the original paper by Patel et al. [4]. The first issue is with regards to the pH and lactic acid conversion. The author uses lactic acid concentration as well as pH at various points within the original paper without linking the two. There is no conversion scale between the two except for a mention that a lactic acid concentration of $3.98 \cdot 10^{-5} mM$ corresponds to a pH of 7.4. We had to make a few physiologically incorrect assumptions in order to make the model work. These were to assume lactic acid secretion by tumour cells was the only source of hydrogen ions, the hydrogen ions released were not neutralised or buffered and the pKa of lactic acid was constant.

Another problem we faced was with the order of updating the cellular automaton. The author stated that cellular element states were updated after the chemical fields were updated. However, there was no order as to which status changes were updated first and no mention as to whether quiescent cells can turn active. For our simulations, we have assumed that quiescent cells can turn active if the pH is above the threshold for quiescence. It was also not clear from the paper whether cells could divide into the 4 adjacent spaces only or into all 8 neighbouring spaces. In this cellular automata, we have made the choice of division into 4 possible spaces only.

As a result of these problems with the interpretation of the paper, it is very possible that our cellular automata differs considerably from the original by Patel et al. [4]. It is possible, in addition to the problems mentioned above, that different pde solvers were used and this would affect the values of both the chemical fields, leading to the differences in the results seen.

The results of this cellular automata are significantly different from that of the original by Patel et al. [4] For instance, the tumour did not grow in our simulations unless the tumour acid production rate was at least $4.75 \cdot 10^{-5} mM/s$ while it grew even with an acid production rate of $2.5 \cdot 10^{-5} mM/s$ in the original paper. While the trends seen are similar, more differences are also evident in (Figures 3.2a and 3.2b). In Figure 3.2b, the growth rate does not decrease even with a vessel density of 0.20, which is unlike the original where the growth rate decreases when the vessel density is 0.18 or above.

4.2 Biological Significance and Future Work

Our hybrid cellular automaton explores the effects of vessel density and tumour acid production on the growth and development of avascular, early stage tumours. While this is not completely representative of all tumours, it is still a useful model for this purpose as it is able to capture many of the known characteristics of tumour growth and compares well with real life tumours. Our model also allows many parameters to be user defined and this allows any user to adjust any combination of many parameters which include survival and quiescence thresholds of both normal and tumour cells, starting glucose and lactic acid concentrations as well as the size of the initial tumour. This is an improvement on the original automaton and would be useful for investigations where are are different values of these parameters, among others.

Future work on our cellular automaton should include the expansion of this automaton to include parameters for oxygen as well as its diffusion as hypoxia is also an important factor for tumour growth. An angiogenesis simulation can also be included in order to expand the simulation past the avascular growth stage. However, both of these improvements would require further research on the values of parameters required as well as the development of a completely new angiogenesis function.

Bibliography

[1] R.A. Gatenby and E.T. Gawlinski. A reaction-diffusion model of cancer invasion. *Cancer Research*, 56(24):5745–5753, 1996.

[2] J. R. Griffiths. Are cancer cells acidic? *Br. J. Cancer*, 64(3):425–427, Sep 1991.

[3] P. M. Gullino, F. H. Grantham, A. H. Courtney, and I. Losonczy. Relationship between oxygen and glucose consumption by transplanted tumors in vivo. *Cancer Res.*, 27(6):1041–1052, Jun 1967.

[4] Aalpen A. Patel, Edward T. Gawlinski, Susan K. Lemieux, and Robert A. Gatenby. A cellular automaton model of early tumor growth and invasion: The effects of native tissue vascularity and increased anaerobic tumor metabolism. *Journal of Theoretical Biology*, 213(3):315 – 331, 2001.

[5] J. Rozhin, M. Sameni, G. Ziegler, and B. F. Sloane. Pericellular pH affects distribution and secretion of cathepsin B in malignant cells. *Cancer Res.*, 54(24):6517–6525, Dec 1994.

[6] H. Yamasaki. Aberrant expression and function of gap junctions during carcinogenesis. *Environ. Health Perspect.*, 93:191–197, Jun 1991.